2.8 Million Years of Arctic Climate Change from Lake El'gygytgyn, NE Russia

Martin Melles,[1]* Julie Brigham-Grette,[2] Pavel S. Minyuk,[3] Norbert R. Nowaczyk,[4] Volker Wennrich,[1] Robert M. DeConto,[2] Patricia M. Anderson,[5] Andrei A. Andreev,[1] Anthony Coletti,[2] Timothy L. Cook,[2]† Eeva Haltia-Hovi,[4]‡ Maaret Kukkonen,[1] Anatoli V. Lozhkin,[3] Peter Rosén,[6] Pavel Tarasov,[7] Hendrik Vogel,[1] Bernd Wagner[1]

The reliability of Arctic climate predictions is currently hampered by insufficient knowledge of natural climate variability in the past. A sediment core from Lake El'gygytgyn in northeastern (NE) Russia provides a continuous, high-resolution record from the Arctic, spanning the past 2.8 million years. This core reveals numerous "super interglacials" during the Quaternary; for marine benthic isotope stages (MIS) 11c and 31, maximum summer temperatures and annual precipitation values are ~4° to 5°C and ~300 millimeters higher than those of MIS 1 and 5e. Climate simulations show that these extreme warm conditions are difficult to explain with greenhouse gas and astronomical forcing alone, implying the importance of amplifying feedbacks and far field influences. The timing of Arctic warming relative to West Antarctic Ice Sheet retreats implies strong interhemispheric climate connectivity.

The effects of global warming are documented and predicted to be most pronounced in the Arctic, a region that plays a crucial, but not yet well-understood role within the global climate system (*1*). Reliable climate projections for high northern latitudes are, however, hampered by the complexity of the underlying natural variability and feedback mechanisms (*2*, *3*). To date, information concerning the natural climate variability in the Arctic is widely restricted to the last glacial/interglacial cycle, the period covered by the longest ice-core records from the Greenland ice cap (*4*). A limited number of records extend deeper in time, from both the marine realm (*5*) and the Arctic borderland (*6*), but these records are restricted in terms of age control and temporal resolution.

Here, we present a time-continuous and high-resolution record of environmental history from the Arctic spanning the past 2.8 million years (My) from Lake El'gygytgyn, located ~100 km to the north of the Arctic Circle in northeastern Russia (67.5°N, 172°E) (Fig. 1). The length, temporal continuity, and centennial- to millennial-scale temporal resolution (Fig. 2 and supplementary materials) provide a detailed view of natural climatic and environmental variability in the terrestrial Arctic, a better understanding of the representative nature of the last climate cycle for the Quaternary, and insight into how sensitively the terrestrial Arctic reacts to a range of forcing mechanisms.

Lake setting, drilling, and core analyses. Lake El'gygytgyn is located in a meteorite impact crater formed 3.58 million years ago (Ma) (*7*). The 170-m-deep lake has a bowl-shaped morphology with a diameter of ~12 km, a surface area of 110 km^2, and a relatively small catchment of 293 km^2 (*8*). The modern continental Arctic climate produces herb-dominated tundra in the catchment, 9 months per year of lake-ice cover, and oligotrophic to ultra-oligotrophic conditions in the lake. Low productivity in combination with complete overturning of the water column during the ice-free period in summer leads to well-oxygenated bottom waters throughout the year.

Scientific deep drilling was performed in the El'gygytgyn Crater in winter 2008/2009 (*9*). We used advanced high-resolution (logging/scanning) technologies and standard techniques to investigate the core composite from site 5011-1 (Fig. 1) of the International Continental Scientific Drilling Program (ICDP) for lithology as well as selected physical, chemical, and biological proxies (*10*). According to the age model (Fig. 2), which is based on magnetostratigraphy and tuning of proxy data to the regional insolation and global marine isotope stratigraphy (fig. S1), the upper 135.2 m of the sediment record continuously represents the environmental history of the past 2.8 My. To display the obtained data versus time (Fig. 3) we removed volcanic ashes and other event layers caused by mass movement deposits (*10*). Though highly varied in nature, the resultant record of pelagic sedimentation consists of three dominant lithofacies (see supplementary materials). Climate and environmental interpretation of the pelagic sedimentation record is based on complementary biological and geochemical indicators, which show that distinct facies reflect end-member glacial/interglacial climatic conditions (*9*, *11*).

Glacial variability and proxies. Facies A is characterized by dark gray to black finely laminated (<5 mm) silt and clay and may contain

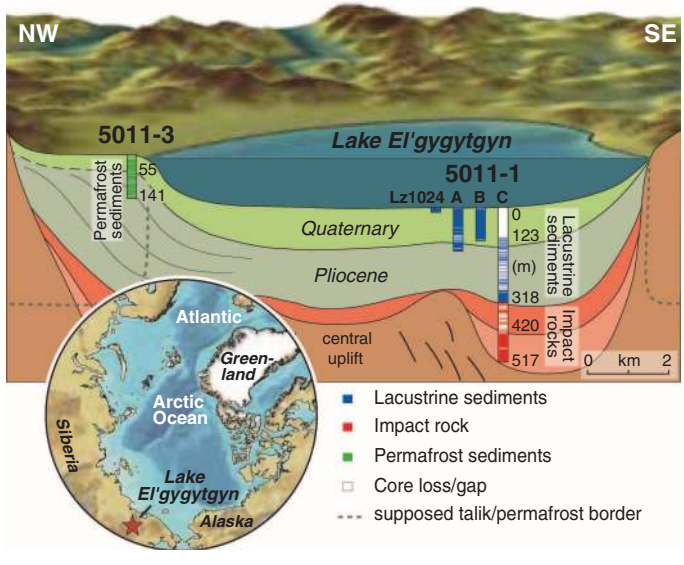

Fig. 1. Location of Lake El'gygytgyn in northeastern Russia (inserted map) and schematic cross-section of the El'gygytgyn basin stratigraphy showing the location of ICDP sites 5011-1 and 5011-3. At site 5011-1, three holes (1A, 1B, and 1C) were drilled to replicate the Quaternary and uppermost Pliocene sections. Hole 1C further penetrated through the remaining lacustrine sequence down to a 318-m depth and then ~200 m into the impact rock sequence underneath. Lz1024 is a 16-m-long percussion piston core taken in 2003 that fills the stratigraphic gap between the lake sediment surface and the top of drill cores 1A and 1B.

[1]Institute of Geology and Mineralogy, University of Cologne, Zuelpicher Strasse 49a, D-50674 Cologne, Germany. [2]Department of Geosciences, University of Massachusetts, 611 North Pleasant Street, Amherst, MA 01003, USA. [3]Far East Branch Russian Academy of Sciences, North-East Interdisciplinary Scientific Research Institute, 16 Portovaya Street, 685000 Magadan, Russia. [4]Helmholtz Centre Potsdam, GFZ German Research Centre for Geosciences, Telegrafenberg C321, D-14473 Potsdam, Germany. [5]Department of Earth and Space Sciences, University of Washington, Box 351310, Seattle, WA 98195–1310, USA. [6]Climate Impacts Research Centre, Umeå University, SE-981 07 Abisko, Sweden. [7]Institute of Geological Sciences, Free University Berlin, Malteserstrasse 74-100, Haus D, D-12249 Berlin, Germany.

*To whom correspondence should be addressed. E-mail: mmelles@uni-koeln.de

†Present address: Department of Physical and Earth Sciences, Worcester State University, Worcester, MA 01602, USA.

‡Present address: Department of Geology, Lund University, Sölvegatan 12, S-223 62 Lund, Sweden.

elongated sediment clasts of coarser grain sizes (fig. S2). This facies was deposited during times of heavy global marine isotopic values (*12*) and low regional July insolation (Fig. 3, A, B, and D) (*13*). Facies A represents peak glacial conditions, when perennial lake ice persisted, requiring mean annual air temperatures at least 4 (± 0.5)°C lower than today (*14*). This resulted in a stagnant water column with oxygen-depleted bottom waters, as reflected by low Mn/Fe ratios (Fig. 3G) and minima in magnetic susceptibility (MS) (Fig. 3E), indicating reducing conditions with magnetite dissolution (see supplementary materials). Dark laminations along with maxima in the content of total organic carbon (TOC) (Fig. 3F) reflect the absence of bioturbation and enhanced preservation of organic matter. Low Si/Ti ratios (Fig. 3H) and a robust correlation between Si/Ti ratios and biogenic silica contents (see supplementary materials), however, suggest relatively low primary production.

Facies A first appears 2.602 to 2.598 Ma, during marine isotope stage (MIS) 104 (Fig. 3D), corresponding with pollen assemblages that indicate substantial cooling at the Pliocene/Pleistocene boundary (see supplementary materials). This cooling coincides with distinct climatic deterioration at Lake Baikal (*15*) and may be associated with the poorly dated Okanaanean Glaciation in eastern Chukotka at the beginning of the Pleistocene (*16*). On the other hand, the first occurrence of facies A at Lake El'gygytgyn clearly postdates the onset of stratification across the western subarctic Pacific Ocean at 2.73 Ma, an event believed to have triggered the intensification of Northern Hemispheric glaciation (*17*). Hence, the onset of full glacial cycles in central Chukotka cannot directly be linked to changes in thermohaline circulation in the Pacific.

From the long-term succession of facies A (Fig. 3D) and Mn/Fe ratios (Fig. 3G), pervasive glacial episodes at Lake El'gygytgyn gradually increase in frequency from ~2.3 to ~1.8 Ma, eventually concurring with all glacials and several stadials reflected globally in stacked marine isotope records (*12*). The full establishment of glacial/interglacial cycles by ~1.8 Ma at Lake El'gygytgyn coincides well with enhanced glacial erosion in British Columbia (*18*) and the onset of subpolar cooling in both hemispheres with an average bipolar temperature drop of 4° to 5°C due to the emergence of the tropical Pacific cold tongue (*19*). Nevertheless, this event clearly predates the mid-Pleistocene transition, when the dominance of 41 thousand years (ky) of obliquity was globally replaced by the 100-ky cycle between 1.25 and 0.7 Ma (*20*).

Interglacial variability and proxies. Facies B is characterized by massive to faintly banded silt that is olive gray to brownish in color (fig. S2). This facies comprises the majority of sediment that accumulated in Lake El'gygytgyn during the past 2.8 My, representing 79% of the Quaternary history (Fig. 3D). Facies B reflects a wide range of glacial to interglacial settings and includes the style of modern sedimentation. As such, a seasonal ice cover promotes higher diatom productivity, as indicated by high Si/Ti ratios (Fig. 3H and supplementary materials). In contrast, TOC content is low (Fig. 3F), suggesting high organic matter decomposition due to oxygenation of bottom waters as a consequence of wind- and density-driven mixing. Complete water-column ventilation is also indicated in the sediment colors, maxima in MS (Fig. 3E), and high Mn/Fe ratios (Fig. 3G). In addition, the lack of stratification indicates minor sediment homogenization by bioturbation.

Facies C consists of reddish-brown silt-sized sediment with distinct fine laminations (<5 mm) (fig. S2). This facies is irregularly distributed in the record compared with facies A and B (Fig. 3D). Facies C coincides with some periods of light values in the global marine isotope record and high regional July insolation (Fig. 3, A and B). The characteristics of facies C suggest that it represents particularly warm interglacials. High Mn/Fe ratios (Fig. 3G) along with reddish-brown sediment colors imply well-oxygenated bottom waters. In contrast with facies B, however, the sediments are distinctly laminated. This is traced back to a combination of factors, including a particularly high primary production in spring and summer and anoxic bottom water conditions during winter stratification under a seasonal ice cover, which excludes bioturbation despite annual oxygenation. High primary production, presumably caused by a longer ice-free season and enhanced nutrient supply from the catchment relative to other interglacials, is indicated by exceptionally high Si/Ti ratios (Fig. 3H). Anoxic bottom water

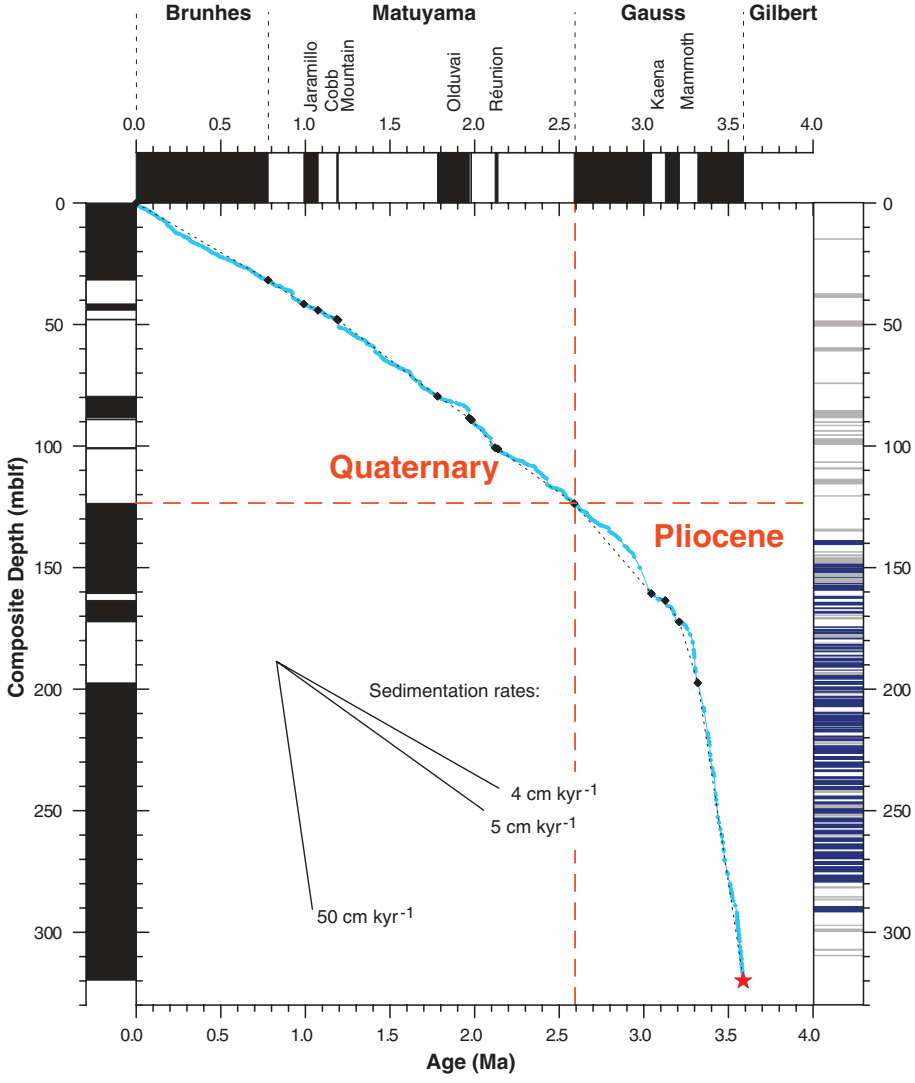

Fig. 2. Age/depth model with resulting sedimentation rates for the ICDP 5011-1 core composite based on magnetostratigraphy and correlation between sediment proxy data, the LR04 marine isotope stack (*12*), and regional spring and summer insolation (*13*). Initial first-order tie points are indicated by black diamonds; second- and third-order tie points are denoted by the blue curve. The red star marks the time of the impact inferred from $^{40}Ar/^{39}Ar$ dating (*7*) at 3.58 (±0.04) Ma. Black and white bars denote normal and reversed polarity, respectively. Mass movement deposits and core gaps greater than 50 cm in thickness are indicated on the right *y* axis in gray and blue, respectively. mblf, meters below lake floor.

conditions during winter are implied by high TOC contents (Fig. 3F), reflecting high primary production and incomplete decomposition compared with facies B, and variable MS values (Fig. 3E), reflecting partial dissolution of magnetite.

The described characteristics of facies C are most pronounced for MIS 11c, 31, 49, 55, 77, 87, 91, and 93 (red bars in Fig. 3), suggesting that these interglacials represent unusual "super interglacials" in the Arctic throughout the Quaternary. The exceptional character of these interglacial conditions becomes evident based on a comparison of MIS 1 and 5e (facies B) with MIS 11c and 31 (super interglacials of facies C), using additional biological proxies and pollen-based climate reconstructions (Fig. 3, I to L).

Sediments formed in Lake El'gygytgyn during MIS 1 and 5e have Si/Ti ratios only slightly higher than those formed during glacial and stadial conditions of MIS 2, 5d, and 6 (Fig. 3K). Pollen data show distinct increases in tree and

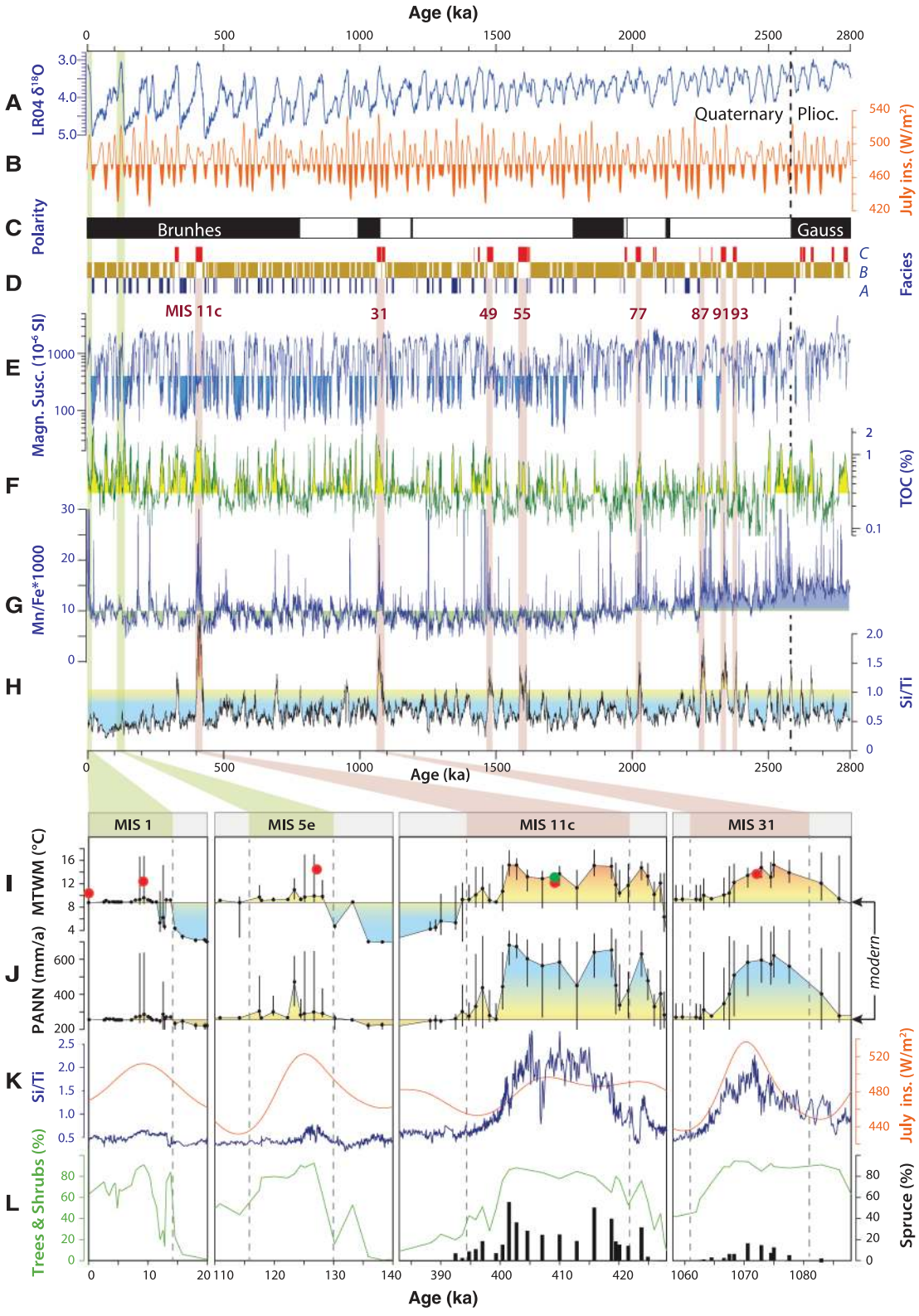

Fig. 3. (**A** to **H**) (A) LR04 global marine isotope stack (*12*) and (B) mean July insolation for 67.5°N (*13*) for the past 2.8 My compared with (C) magnetostratigraphy, (D) facies, (E) magnetic susceptibility, (F) TOC contents, (G) Mn/Fe ratios, and (H) Si/Ti ratios in the sediment record from Lake El'gygytgyn (magnetic susceptibility and x-ray fluorescence data are smoothed using a 500-year weighted running mean to improve the signal-to-noise ratio). Super interglacials at Lake El'gygytgyn are highlighted with red bars. (**I** to **L**) Expanded views into the interglacials MIS 1, 5e, 11c, and 31 and adjoining glacials/stadials. (I) Reconstructed MTWM and (J) PANN based on the pollen spectra and best modern analog approach [modern values from (*56*)]. (K) Mean July insolation for 67.5°N (*13*) compared with El'gygytgyn Si/Ti ratios, smoothed by five-point weighted running mean. (L) Tree and shrub pollen percentages compared with spruce pollen content. Simulated July surface air temperatures (red and green dots) at the location of the lake are shown for comparison. The location of the dots relative to the *x* axis corresponds with the GHG and orbital forcing used in each interglacial simulation (see supplementary materials). Simulated modern and preindustrial temperatures are close to observed values, so model temperatures are not corrected for bias. The green dot indicates the results derived with a deglaciated Greenland and increased heat flux under Arctic Ocean sea ice by 8 W m^{-2}.

shrub pollen (Fig. 3L) and suggest that birch and alder shrubs dominated the vegetation (fig. S4). Pollen-based climate reconstructions (see supplementary materials) suggest that the mean temperature of the warmest month (MTWM; i.e., July) and the annual precipitation (PANN) during the peak of MIS 1 and 5e were only ~1° to 2°C and, with one exception, ~50 mm higher than today, respectively (Fig. 3, I and J).

This observation is consistent with temperature reconstructions for the Holocene thermal maximum, which indicate +1.6 (±0.8)°C warming in the western Arctic (*21*) and +1.7 (±0.8)°C across the entire Arctic (*3*) relative to modern, confirming that Lake El'gygytgyn records regional rather than just local climate change (*14*). In contrast, temperature reconstructions for the MIS 5e thermal maximum are more variable, indicating +5 (±1)°C across the entire Arctic, albeit with smaller anomalies reconstructed for the Pacific sector (*3*, *22*). The warmer climate across the Arctic during MIS 5e compared with MIS 1 is thought to have caused a size reduction of the Greenland Ice Sheet equivalent to 1.6 to 2.2 m in global sea-level rise (*23*).

Strongly enhanced primary productivity during the super interglacials MIS 11c and 31 compared with MIS 1 and 5e, as inferred from higher Si/Ti ratios (Fig. 3K), is associated with comparable maxima in tree and shrub pollen but is marked by distinct differences in pollen composition (Fig. 3L and supplementary materials). For instance, substantial spruce pollen is present during MIS 11c and 31 but is missing during shrub-dominated MIS 1 and 5e interglacials. According to the best modern analog (BMA; see supplementary materials) climate reconstruction, maximum MTWM and PANN were up to 4° to 5°C and ~300 mm higher than those of MIS 1 and 5e, respectively (Fig. 3, I and J).

Sediment records of MIS 11 are rare in the Arctic, and their reconstructed temperature signals are inconclusive (*22*). However, there are indications that the Greenland Ice Sheet was much smaller or even absent (*24*, *25*), with forests covering at least South Greenland (*26*). Relative sea level may have been significantly higher than today (*25*, *27*). Particularly warm conditions are also suggested by records from Lake Biwa (*28*), Lake Baikal (*29*), the mid-latitude Atlantic (*30*), and the Belize Reef (*31*) and may have been associated with megadroughts in the southwestern United States (*32*).

As yet, MIS 31 is not unambiguously recorded in the Arctic, but it is known for substantial changes in and around Antarctica, including a southward shift of the subtropical front and warmer waters in the Southern Ocean (*33*, *34*) and the collapse of the West Antarctic Ice Sheet (WAIS) (*35*). In the Northern Hemisphere, the Plio/Pleistocene Gubik Formation of northern Alaska includes at least five sea-level high stands associated with episodes of warm climate and reduced sea ice (*36*). One of these episodes, the Fishcreekian transgression, is now thought to have occurred ~1.2 Ma (*37*) and thus may be correlative with MIS 31. Another possibly correlative site is at Fosheim Dome on Ellesmere Island. This site includes terrestrial deposits dated to ~1.1 Ma, which enclose fossil beetle (Coleoptera) assemblages, suggesting temperatures 8° to 14°C above modern values (*38*).

Other Arctic sites potentially correlative with one or more of the older Early Pleistocene super interglacials recorded in Lake El'gygytgyn (Fig. 3) include the Kap København Formation in northern Greenland, currently dated to ~2.4 Ma. At this time, sea ice was strongly reduced and forests reached the Arctic Ocean about 1000 km further to the north than today (*39*). Another candidate is the balmy Bigbendian Transgression of the Gubik Formation dated to ~2.6 Ma (*36*).

Interglacial forcings and feedbacks. Comparing the relative warmth of the Pleistocene interglacials recorded at Lake El'gygytgyn (Fig. 3I) in the context of orbital and greenhouse gas (GHG) forcing (*40*), we find that peak summer warmth during MIS 5e and 31 corresponds to the congruence of high obliquity, high eccentricity, and precession aligning perihelion with boreal summer. The net effect of this orbital configuration produces high-intensity summer insolation at the lake, >50 Wm^{-2} greater than today (Fig. 3K). Similarly, peak warmth during MIS 1 and 11c also coincides with perihelion during boreal summer, but lower eccentricity (and lower obliquity at MIS 11c) attenuates the effect of precession relative to MIS 5e and 31, making summer insolation forcing less intense, albeit longer in duration.

GHG radiative forcing from a combination of CO_2, CH_4, and N_2O atmospheric mixing ratios determined from ice cores (see supplementary materials) is similar during MIS 5e and 11c (+0.16 and +0.19 Wm^{-2} relative to preindustrial GHG concentrations, respectively). Early MIS 1 is clearly an exception, with substantially lower CO_2 levels [~260 parts per million by volume (ppmv)] around the time of peak Holocene warmth [~9 thousand years ago (ka)] producing −0.44 Wm^{-2} less radiative forcing relative to preindustrial levels. MIS 31 (~1.072 Ma) lies beyond the oldest ice cores, so no direct information on atmospheric composition is available. However, a proxy-based reconstruction of mid-Pleistocene partial pressure of CO_2 based on boron isotopes in plank-

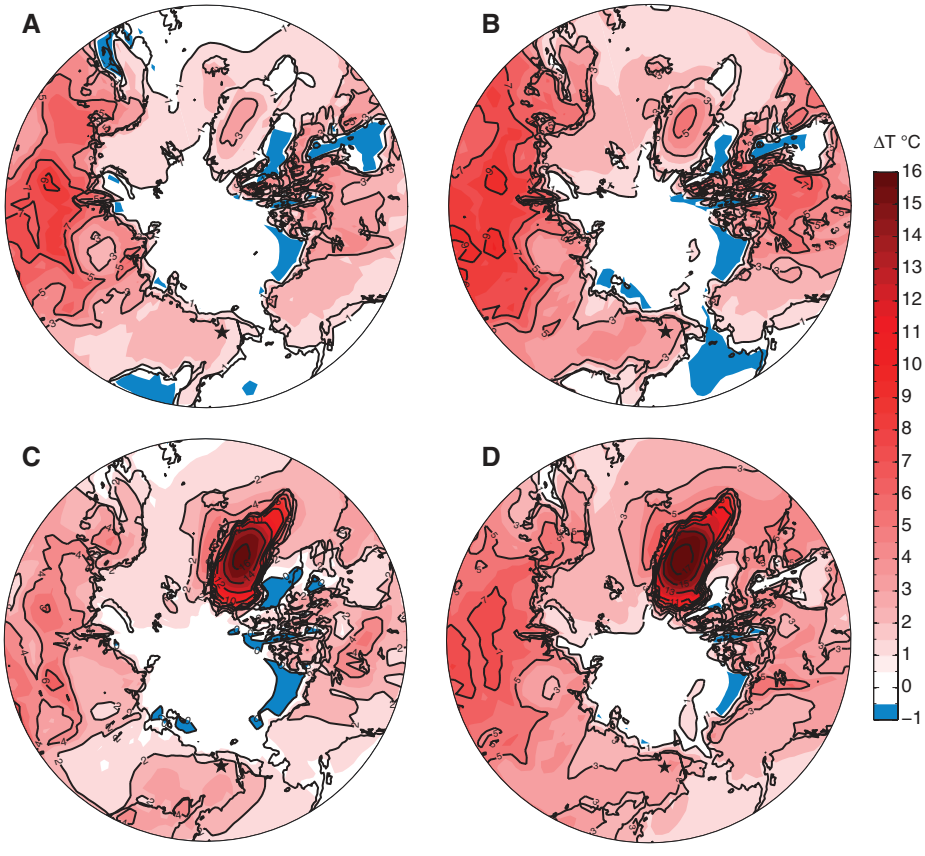

Fig. 4. Simulated interglacial warming (2-m surface temperature in degrees Celsius) relative to preindustrial levels. (**A**) MIS 1 (9-ky orbit and GHGs). (**B**) MIS 5e (127-ky orbit and GHGs). (**C**) MIS 11c (409-ky orbit, GHGs, no Greenland Ice Sheet, and 8 W m^{-2} enhanced oceanic heat convergence under Arctic sea ice). (**D**) MIS 31 (1072-ky orbit, GHGs, and no Greenland Ice Sheet). Orbital and GHG forcing for MIS 5e and 11c follow that used by Yin and Berger (*40*). Forcing for MIS 31 follows that used by DeConto *et al.* (*42*). The location of Lake El'gygytgyn is shown with a star near the bottom-center of each panel. Areas of no shading (white) roughly correspond to statistically insignificant anomalies at the 95% confidence interval.

tonic foraminifera (*41*) indicates that the highest mid-Pleistocene CO_2 levels (~325 ppmv) occurred around 1 Ma, roughly coinciding with the exceptional warmth of MIS 31. Though uncertain, these reconstructed CO_2 levels at MIS 31 would have added ~0.84 Wm^{-2} of radiative forcing, even if CH_4 and N_2O mixing levels remained close to preindustrial values, which is unlikely considering the ubiquitous correlation of elevated CH_4 and N_2O during late Pleistocene interglacials. In sum, much of the warmth during MIS 31 can be explained by elevated greenhouse gas levels (*42*).

To investigate potential reasons for the super interglacials at Lake El'gygytgyn, we tested the equilibrated response of a Global Climate Model (GCM) with an interactive vegetation component (see supplementary materials) to the orbital and GHG forcing corresponding to the timing of peak summer warmth at MIS 1, 5e, 11c, and 31. Comparisons with a preindustrial control simulation (Fig. 4) show that differences in MTWM maxima at Lake El'gygytgyn during MIS 1 and 5e (+2.1° and +4.2°C) were in the same range as those during MIS 11c and 31 (+2.2° and +3.5°C) (Fig. 3I, red dots, Fig. 4, and supplementary materials). The same holds true for the modeled differences in PANN (0 and –37 mm/a and +38 and 0 mm/a, respectively). The results are similar to previous interglacial simulations using an intermediate complexity model (*40*), with the combined effect of orbital and GHG forcing at MIS 5e producing the greatest summer warming among the four interglacials modeled here. Our simulated summer warming (4.2°C) over the Beringian interior at MIS 5e also closely matches the warming simulated by a coupled atmosphere-ocean GCM (*43*). Consequently, the distinctly higher observed values of MTWM and PANN at MIS 11c cannot readily be explained by the local summer orbital forcing or GHG concentrations alone and suggest that other processes and feedbacks contributed to the extraordinary warmth at this interglacial and the relatively muted response to the strongest forcing at MIS 5e.

Vegetation-land surface feedbacks are accounted for in our model, and the simulated poleward advance of evergreen needle-leaf forest during the interglacials provides a good match with our reconstructions (see supplementary materials), yet the warming effect of boreal forest expansion does not provide a satisfactory explanation for the warmth of MIS 11c. A deglaciated Greenland has been shown to have important regional effects on surrounding sea surface temperatures (SSTs) and sea-ice conditions, but widespread warming in the circum-Arctic (and Beringia in particular) has been shown to be minimal (*43*, *44*). This observation is supported by our simulations, showing that the loss of the Greenland Ice Sheet at MIS 11c raises summer temperatures at Lake El'gygytgyn by only 0.3°C. Furthermore, Greenland was likely reduced in size during MIS 5e and perhaps other interglacials, offering little help in differentiating Beringia's response from one interglacial to the next. Meltwater impacts on ocean overturning (ignored in our simulations) generally have a cooling effect on the Northern Hemisphere, adding to the difficulty in explaining the exceptional warmth at MIS 11c relative to MIS 1 and 5e.

The super interglacials at Lake El'gygytgyn coincide remarkably with diatomite layers in the Antarctic ANDRILL 1B record (see supplementary materials), which reflect periods of a diminished WAIS and open water in the Ross Embayment (*35*, *45*). The higher number of events at Lake El'gygytgyn does not necessarily reflect a higher frequency, but it may also reflect the discontinuity of the ANDRILL 1B record (*46*).

Linkages between extraordinary warmth at Lake El'gygytgyn and Antarctic ice volume imply strong intrahemispheric climate coupling that could be related to reductions in Antarctic Bottom Water (AABW) formation (*47*) during times of ice sheet/shelf retreat and elevated fresh water input into the Southern Ocean. This is supported by distinct minima in AABW inflows into the southwest Pacific during MIS 11 and 31 (*48*). As a consequence, changes in thermohaline circulation during MIS 11 and 31 might have reduced upwelling in the northern North Pacific (*49*), as indicated by distinctly lower BSi concentrations compared with other interglacials at Ocean Drilling Program site 882 (*50*, *51*). A stratified water column during the super interglacials would have resulted in higher SSTs in the northern North Pacific, with the potential to raise air temperatures and precipitation rates over adjacent land masses via effects on the dominant pressure patterns (Siberian high and Aleutian low) that dominate the modern climatology at the lake (*52*).

An alternative mechanism linking Lake El'gygytgyn with Antarctica could be related to higher relative sea level due to the combined retreats of the WAIS (*44*) and the Greenland Ice Sheet (*24*), resulting in enhanced warm-water intrusion into the Arctic Ocean. Potential gateways are the Denmark Strait and Barents Sea from the Atlantic Ocean and the Bering Strait from the Pacific Ocean. In the northeastern Atlantic, however, SSTs, at least during MIS 11, were lower than during MIS 9, 5e, and 1 (*53*). Today, Bering Strait throughflow is restricted by shallow waters of only ~50 m in depth, resulting in an average northward transport of ~0.8 sverdrups (1 sverdrup = 10^6 m^3 s^{-1}) (*54*). Substantial interannual variability in flow rate can produce elevated heat fluxes (5 to 6 × 10^{20} J/year in 2007), which can be amplified in the Arctic by internal-feedback mechanisms (*3*). No evidence as yet exists for substantial changes in temperature or flow rates during super interglacials; however, as a first exploration of this idea, we increased the heat flux convergence under Arctic sea ice in our interglacial climate model simulations by 8 W m^{-2} (reflecting an extreme ~fourfold increase in warmer Bering Strait throughflow). The additional heat flux results in substantial reductions in seasonal sea ice and warmer Arctic SSTs but contributes little additional warming (<0.7°C) (Figs. 3I and 4C) in the Beringian interior.

Fully testing these ideas will require additional climate-ocean modeling, explicitly accounting for glacial/interglacial changes in regional sea level (paleobathymetry and gateways), changes in land-ice distributions, and melt-water inputs in both polar regions, as well as contemporaneous sediment records from the Arctic and North Pacific Oceans.

The paleoclimatic record from Lake El'gygytgyn provides a benchmark of Arctic change from an area that has otherwise been a data desert for time-continuous terrestrial records of the Pliocene and Pleistocene. The sediments provide a fresh window into the environmental dynamics of the Arctic from a terrestrial high-latitude site for comparison with other Arctic records. Marine cores from the Arctic basin, such as those from the ACEX/Lomonosov Ridge or HOTRAX expeditions (*55*), still lack the comparable resolution and length to test for perennial versus seasonal sea-ice conditions during interglacials over the past 2.8 My. The attenuated response of Arctic SSTs in model simulations of the interglacials (Fig. 4) (*43*) relative to surrounding continents hints that deep Arctic Ocean cores might not provide a complete perspective of the pacing or magnitude of climate change in the Arctic borderlands. The observed response of the region's climate and terrestrial ecosystems to a range of interglacial forcing provides a challenge for modeling and important constraints on climate sensitivity and polar amplification. The marked coherence of interglacial warmth across the western Arctic with repeated deglaciation events in West Antarctica supports the notion of strong teleconnections between the polar regions over the past 2.8 My.

References and Notes

1. ACIA, *Arctic Climate Impact Assessment* (Cambridge Univ. Press, Cambridge, 2005).
2. J. Christensen *et al.*, in *Fourth Assessment Report of the Intergovernmental Panel on Climate Change* (Cambridge Univ. Press, Cambridge, 2007), pp. 847–940.
3. G. H. Miller *et al.*, *Quat. Sci. Rev.* **29**, 1779 (2010).
4. North Greenland Ice Core Project members, *Nature* **431**, 147 (2004).
5. M. O'Regan, C. J. Williams, K. E. Frey, M. Jakobsson, *Oceanography* **24**, 66 (2011).
6. CAPE Last Interglacial Project Members, *Quat. Sci. Rev.* **25**, 1383 (2006).
7. P. Layer, *Meteorit. Planet. Sci.* **35**, 591 (2000).
8. M. Nolan, J. Brigham-Grette, *J. Paleolimnol.* **37**, 17 (2007).
9. M. Melles *et al.*, *Sci. Drill.* **11**, 29 (2011).
10. Materials and methods are available as supplementary materials on *Science* Online.
11. M. Melles *et al.*, *J. Paleolimnol.* **37**, 89 (2007).
12. L. E. Lisiecki, M. E. Raymo, *Paleoceanography* **20**, PA1003 (2005).
13. J. Laskar *et al.*, *Astron. Astrophys.* **428**, 261 (2004).
14. M. Nolan, *Clim. Past Disc.* **8**, 1443 (2012).
15. D. Demske, B. Mohr, H. Oberhänsli, *Palaeogeogr. Palaeoclimatol. Palaeoecol.* **184**, 107 (2002).
16. A. F. Fradkina *et al.*, *Geol. Soc. Am. Spec. Pap. 382* (2005).
17. G. H. Haug *et al.*, *Nature* **433**, 821 (2005).
18. D. L. Shuster, T. A. Ehlers, M. E. Rusmoren, K. A. Farley, *Science* **310**, 1668 (2005).
19. A. Martínez-Garcia, A. Rosell-Melé, E. L. McClymont, R. Gersonde, G. H. Haug, *Science* **328**, 1550 (2010).

20. P. U. Clark *et al*., *Quat. Sci. Rev.* **25**, 3150 (2006).
21. D. S. Kaufman, J. Brigham-Grette, *Quat. Sci. Rev.* **12**, 21 (1993).
22. G. H. Miller *et al*., *Quat. Sci. Rev.* **29**, 1679 (2010).
23. E. J. Colville *et al*., *Science* **333**, 620 (2011).
24. E. Willerslev *et al*., *Science* **317**, 111 (2007).
25. M. E. Raymo, J. X. Mitrovica, *Nature* **483**, 453 (2012).
26. A. de Vernal, C. Hillaire-Marcel, *Science* **320**, 1622 (2008).
27. G. A. Milne, J. X. Mitrovica, *Quat. Sci. Rev.* **27**, 2292 (2008).
28. P. E. Tarasov *et al*., *Earth Sci. Rev.* **108**, 64 (2011).
29. A. A. Prokopenko *et al*., *Clim. Past* **6**, 31 (2010).
30. R. Stein, J. Hefter, J. Grützner, A. Voelker, B. D. A. Naafs, *Paleoceanography* **24**, PA2203 (2009).
31. E. Gischler, R. N. Ginsburg, J. O. Herrle, S. Prasad, *Sedimentology* **57**, 1049 (2010).
32. P. J. Fawcett *et al*., *Nature* **470**, 518 (2011).
33. R. P. Scherer *et al*., *Geophys. Res. Lett.* **35**, L03505 (2008).
34. P. Maiorano, M. Marino, J.-A. Flores, *Mar. Micropaleontol.* **71**, 166 (2009).
35. T. Naish *et al*., *Nature* **458**, 322 (2009).
36. J. Brigham-Grette, L. D. Carter, *Arctic* **43**, 74 (1992).
37. G. A. Goodfriend, J. Brigham-Grette, G. H. Miller, *Quat. Res.* **45**, 176 (1996).
38. S. A. Elias, J. V. Matthews Jr., *Can. J. Earth Sci.* **39**, 911 (2002).
39. S. Funder *et al*., *Bull. Geol. Soc. Den.* **48**, 177 (2001).
40. Q. Z. Yin, A. Berger, *Clim. Dyn.* **36**, 1 (2011).
41. B. Hönisch, N. G. Hemming, D. Archer, M. Siddall, J. F. McManus, *Science* **324**, 1551 (2009).
42. R. M. DeConto, D. Pollard, D. Kowalewski, *Global Planet. Change* **88-89**, 45 (2012).
43. B. L. Otto-Bliesner *et al*., *Science* **311**, 1751 (2006).
44. S. J. Koenig, R. M. DeConto, D. Pollard, *Clim. Dyn.* **37**, 1247 (2011).
45. D. Pollard, R. M. DeConto, *Nature* **458**, 329 (2009).
46. R. McKay *et al*., *Quat. Sci. Rev.* **34**, 93 (2012).
47. A. Foldvik, *J. Geophys. Res.* **109**, C02015 (2004).
48. I. R. Hall, I. N. McCave, N. J. Shackleton, G. P. Weedon, S. E. Harris, *Nature* **412**, 809 (2001).
49. E. D. Galbraith *et al*., *Nature* **449**, 890 (2007).
50. G. H. Haug, M. A. Maslin, M. Sarnthein, R. Stax, R. Tiedemann, *Proc. ODP Sci. Results* **145**, 293 (1995).
51. S. L. Jaccard, E. D. Galbraith, D. M. Sigman, G. H. Haug, *Quat. Sci. Rev.* **29**, 206 (2010).
52. C. J. Mock, P. J. Bartlein, P. A. Anderson, *Int. J. Climatol.* **18**, 1085 (1998).
53. J. P. Helmke, H. A. Bauch, *Paleoceanography* **18**, 1036 (2003).
54. R. A. Woodgate, T. Weingartner, R. Lindsay, *Geophys. Res. Lett.* **37**, L01602 (2010).
55. L. Polyak, M. Jakobsson, *Oceanography* **24**, 52 (2011) and references therein.
56. M. New, D. Lister, M. Hulme, I. Makin, *Clim. Res.* **21**, 1 (2002).

Acknowledgments: Drilling operations were funded by the ICDP, the NSF, the German Federal Ministry of Education and Research (BMBF), Alfred Wegener Institute and Helmholtz Centre Potsdam (GFZ), the Russian Academy of Sciences Far East Branch, the Russian Foundation for Basic Research, and the Austrian Federal Ministry of Science and Research. The Russian Global Lake Drilling 800 drilling system was developed and operated by DOSECC. We thank all participants of the expedition for their engagement during recovery of the ICDP 5011-1 cores. Funding of core analyses was provided by BMBF (grant 03G0642), German Research Foundation (Deutsche Forschungsgemeinschaft, grants ME 1169/21 and ME 1169/24), the NSF (grant 0602471), Vetenskapsrådet, The Swedish Research Council, the Kempe Foundation, and the Civilian Research and Development Foundation (grant RUG1-2987-MA-10). We thank N. Mantke, A. Shahnazarian, and numerous students (Univ. of Cologne) for their competent help in core processing; T. Matrosova for contributing modern surface pollen data; and R. McKay for providing a modified lithological log of the ANDRILL 1B record. We also thank four anonymous reviewers for supportive and constructive comments that greatly improved the manuscript. The data reported in this paper are available in the databases of PANGAEA via www.pangaea.de (DOI: 10.1594/PANGAEA.783305) and of the U.S. National Climatic Data Center via www.ncdc.noaa.gov/paleo/paleolim/paleolim_data.html.

Supplementary Materials

www.sciencemag.org/cgi/content/full/science.1222135/DC1
Materials and Methods
Supplementary Text
Figs. S1 to S6
Tables S1 to S5
References (*57*–*106*)

19 March 2012; accepted 1 June 2012
Published online 21 June 2012;
10.1126/science.1222135

REPORTS

Imaging the Impact of Single Oxygen Atoms on Superconducting $Bi_{2+y}Sr_{2-y}CaCu_2O_{8+x}$

Ilija Zeljkovic,[1] Zhijun Xu,[2] Jinsheng Wen,[2] Genda Gu,[2] Robert S. Markiewicz,[3] Jennifer E. Hoffman[1]*

High-temperature cuprate superconductors display unexpected nanoscale inhomogeneity in essential properties such as pseudogap energy, Fermi surface, and even superconducting critical temperature. Theoretical explanations for this inhomogeneity have ranged from chemical disorder to spontaneous electronic phase separation. We extend the energy range of scanning tunneling spectroscopy on $Bi_{2+y}Sr_{2-y}CaCu_2O_{8+x}$, allowing a complete mapping of two types of interstitial oxygen dopants and vacancies at the apical oxygen site. We show that the nanoscale spatial variations in the pseudogap states are correlated with disorder in these dopant concentrations, particularly that of apical oxygen vacancies.

Many of today's prominent materials, such as high–transition temperature (T_c) superconductors, doped semiconductors, and colossal magnetoresistance materials, are nonstoichiometric and electronically inhomogeneous at the nanoscale (*1*). Both desirable and undesirable electronic properties may arise from chemical inhomogeneity. To fully understand and harness these materials, and to drive the discovery of new materials, it is crucial to understand the impact of single atoms on these inhomogeneous electronic states.

Cuprate superconductors are quasi–two-dimensional (2D) materials that arise from off-stoichiometric doping of a Mott insulator by oxygen intercalation and/or cation substitution. Nanoscale electronic inhomogeneity in the cuprates has been predicted (*2*, *3*) and detected (*4*–*7*), but the roles of spontaneous electronic phase separation (*2*) and chemical disorder (*3*) are unresolved. Scanning tunneling microscopy (STM) has thus far lacked the necessary energy range to image the full set of relevant dopants. We present atomically resolved STM spectroscopy on $Bi_{2+y}Sr_{2-y}CaCu_2O_{8+x}$ (BSCCO) that doubles the energy range of previous work (*8*) and demonstrates the impact of single dopant atoms on electronic states.

In BSCCO, a prominent gap in the density of states shows energy variation of ~100%, on a 2- to 3-nm length scale, across a wide range of doping (*9*). Recent studies (*10*, *11*) suggest that this spectral inhomogeneity results primarily from variations in the pseudogap (PG), a depression in the density of states near the Fermi level ε_F that persists far above the superconducting T_c, most dominantly on the underdoped side of the phase diagram. Nanoscale variation in the PG offers the opportunity to uncover the variable(s) determining its local strength, thus setting the stage for control of this mysterious phase, whose energy scale anticorrelates with superconductivity (*12*, *13*) and which many believe is a competitor to superconductivity (*11*, *14*).

Several previous studies searched for chemical origins of spectral gap variation in BSCCO. Kinoda *et al*. observed atomic defects in Pb-doped BSCCO with resonance energy +1.7 eV, identified as Bi^{3+} substitutions at the Sr^{2+} site (*15*). These defects may correlate weakly with regions of large PG, but no quantitative analysis was presented (*16*). McElroy *et al*. observed localized conductance signatures in BSCCO at −0.96V, identified as interstitial oxygen dopants (*8*), but several mysteries were left unresolved. First, the counted oxygen fell ~50% short of the expected density for each T_c (*17*). Second, the correlation

[1]Department of Physics, Harvard University, 17 Oxford Street, Cambridge, MA 02138, USA. [2]Condensed Matter Physics and Materials Science Department, Brookhaven National Laboratory, Upton, NY 11973–5000, USA. [3]Department of Physics, Northeastern University, 360 Huntington Avenue, Boston, MA 02115, USA.

*To whom correspondence should be addressed: jhoffman@physics.harvard.edu